

Electropolymerization of Aniline onto Anodic WO_3 Film: An Approach to Extend Polyaniline Electroactivity Beyond pH 7

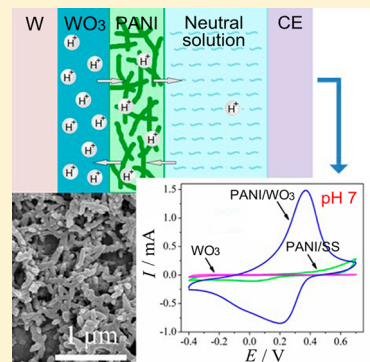
Zejun Chen,^{†,‡} Huiling Lv,^{†,‡} Xufei Zhu,[†] Dongdong Li,^{*,‡} Shaoyu Zhang,[†] Xiaoyuan Chen,[‡] and Ye Song^{*,†}

[†]Key Laboratory of Soft Chemistry and Functional Materials of Education Ministry, Nanjing University of Science and Technology, Nanjing 210094, China

[‡]Shanghai Advanced Research Institute, Chinese Academy of Sciences, 99 Haik Road, Zhangjiang Hi-Tech Park, Pudong, Shanghai 201210, China

S Supporting Information

ABSTRACT: Generally, the redox activity of polyaniline (PANI) can only be retained in acidic media at $\text{pH} < 3$. This high acidity requirement has been a large obstacle in many applications such as biosensor, marine antifouling, and anticorrosion. In this study, composite film systems of PANI and tungsten trioxide (WO_3) were fabricated by the electropolymerization of aniline onto anodic WO_3 film. For the first time, we found that the prepared PANI/ WO_3 film possesses excellent electrochemical activity and cycling stability in neutral solutions. The morphology and composition of the PANI/ WO_3 films were characterized by scanning electron microscope (SEM), X-ray diffraction (XRD), Fourier transform infrared spectroscopy (FT-IR), and X-ray photoelectron spectroscopy (XPS), whereas their electroactivity was evaluated by cyclic voltammetry. Particularly, the long-term stability of their electroactivity upon cycling was investigated in detail. The good electroactivity and high redox stability of the PANI/ WO_3 films in neutral media can be ascribed to the intercalated H^+ ions into WO_3 film during electropolymerization of aniline. Moreover, the reduced electroactivity of the PANI/ WO_3 films can be recovered readily by cyclic voltammetry in an acidic solution. This study provides a new method to tune the electroactivity of PANI beyond pH 7 and makes PANI a promising candidate for biosensors.



INTRODUCTION

Polyaniline (PANI) is one of the earliest researched and the most well-studied conducting polymers owing to its low cost, easy preparation, high electroactivity, controllable electrical conductivity, and good environmental and thermal stability.^{1,2} So far, PANI has been a promising candidate for the development of various devices, such as dye-sensitized solar cells, electrochromic devices, electrochemical sensors, and supercapacitors.^{3–10} However, at higher pH values, PANI becomes deprotonated and loses its conductivity and redox electroactivity. It is generally believed that PANI can remain electroactive only at $\text{pH} < 3$.¹¹ This greatly restricts its applications in neutral or alkaline environments,^{11,12} for example, biosensor, marine antifouling, and anticorrosion. Numerous research efforts have been exerted in the development of approaches to overcome this limitation. Up to now, two different approaches have been used to tune the electroactivity of PANI toward a high pH environment.¹³ One is to introduce acidic groups into the PANI chains or PANI systems to hinder the deprotonation of its conducting form and thus to preserve its electroactivity at higher pH values. The other is to incorporate conductive nanomaterials into a PANI matrix, which is believed to improve the charge transfer rate across the PANI matrix and facilitate its redox processes. The former includes the sulfonation of the emeraldine base,¹⁴

the homopolymerization of aniline derivatives with acidic ionogenic groups¹⁵ or the copolymerization of aniline and aniline derivatives,^{16,17} and the formation of PANI complexes by doping with macromolecular acids.¹⁸ In contrast, the development of PANI nanocomposites fabricated by doping with carbon nanotubes,¹⁹ graphenes,²⁰ Au nanoparticles,^{12,21} etc., falls into the second strategy. Nonetheless, the majority of these reported methods to maintain electroactivity of PANI at higher pH values are not entirely satisfactory, especially for cycling stability.²² Actually, the stability of PANI electroactivity upon cycling at higher pH values has been rarely considered in the literature.

Recently, hybrid systems based organic conducting polymers and inorganic materials have been widely investigated to improve the properties of conducting polymers due to possible synergistic effect. Among these, the hybrid systems composed of PANI and metal oxide semiconductors such as ZnO ,^{23,24} MnO_2 ,²⁵ WO_3 ,^{26–28} and TiO_2 ,^{29–31} have received considerable attention because of their intriguing properties. For instance, the hybrid films of PANI and WO_3 displayed the enhanced electrocatalytic activity,²⁶ higher cathodic photocurrents,²⁷ or

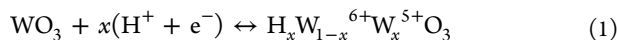
Received: September 13, 2014

Revised: October 30, 2014

Published: November 4, 2014



more impressive electrochromic properties.²⁸ Also, combination of PANI with TiO₂ has led to hybrid materials with advanced catalytic,²⁹ electrochromic,³⁰ and gas-sensing³¹ properties. These studies indicated that the combination of PANI with metal oxides to form inorganic/organic hybrid materials would be an effective approach to improve the electrochemical properties of PANI. However, it is worth noting that for WO₃ and TiO₂ with electrochromic effect, their electrochemical redox process (corresponding to the chromic response) in acidic media was assisted by H⁺ intercalation/deintercalation as charge compensation. For example, in the WO₃ film, the (W⁶⁺/W⁵⁺) redox process is accompanied by the intercalation/deintercalation of H⁺ ions, which can be expressed as follows:^{32,33}



TiO₂ can also undergo a similar redox process.³⁴ Thus, these metal oxides can serve as a host for H⁺ insertion. While introducing the oxides into PANI system, the intercalated H⁺ ions in the oxides may act as proton sources for PANI and make PANI electroactive at higher pH values. More recently, according to this idea, we prepared the PANI hybrid films based on anodic TiO₂ by the electrodeposition of PANI into the TiO₂ nanotubes. The experimental results demonstrated that the hybrid films indeed exhibit an excellent electroactivity and high redox stability in neutral media.³⁵ Obviously, this method to maintain electroactivity of PANI at higher pH values is completely different from the two approaches mentioned above.

In this work, we turned our attention to the composite film systems of PANI and WO₃, which were fabricated by the electropolymerization of aniline onto a WO₃ film. The selection of WO₃ was motivated by the fact that WO₃ may exhibit better H⁺ intercalation behavior and enhanced conductivity owing to the formation of tungsten bronze (H_xWO₃) during the redox process compared with TiO₂.^{33,36} The electroactivity of the PANI film onto WO₃ substrate (designated as PANI/WO₃) at different pH values was investigated by comparing its performance with that of the PANI film onto stainless steel (SS) substrate (designated as PANI/SS). To the best of our knowledge, there is no record in the literature of studying the electroactivity of the PANI/WO₃ films at higher pH values, although their electrochemical properties in acidic media have been investigated intensively. The focus of the present work was on the electroactivity and cycling stability of the PANI/WO₃ films in neutral media. Besides, the underlying mechanism for the high electroactivity of PANI in the PANI/WO₃ systems in neutral media was also suggested.

EXPERIMENTAL SECTION

Anodic Growth of WO₃. Prior to anodization, W foils (0.1 mm thick, 99.95%) were mechanically polished to mirror finish using silicon carbide sandpaper of successively finer roughness (600, 800, 1200, and 2000 grit), and cleaned ultrasonically in two 10 min steps in acetone and deionized water, respectively. WO₃ films were grown in a two-electrode electrochemical cell using the polished W foil as the anode and a graphite rod as the cathode. The anodization electrolyte was 0.1 M HClO₄ aqueous solution whose temperature was kept at 30 °C in a thermostatic water bath. A constant voltage of 50 V was applied for 10 min. Anodizing current transients during anodization were recorded (Figure S1 in the Supporting Information). After

anodization, the resultant WO₃ films were rinsed with deionized water and annealed in air at 450 °C for 3 h at a heating rate of 5 °C min⁻¹.

Fabrication of the Composite Films. All electrochemical experiments were carried out using Autolab potentiostat/galvanostat (PGSTAT302N/FRA2) and Nova software (ver.1.10) in a conventional three-electrode system at room temperature. A saturated calomel electrode (SCE) was used as the reference electrode and a graphite rod as the counter electrode. All potentials are reported with respect to this SCE. The W foils with previously prepared WO₃ films were used as the working electrode, whose area actually exposed to electrolyte was 2 cm². PANI was electrodeposited on WO₃ films by cyclic voltammetry between -0.2 and 1.0 V at a scan rate of 100 mV s⁻¹ from a solution containing 0.1 M aniline and 0.5 M H₂SO₄. The amount of the deposited PANI was controlled by the first anodic peak current that occurred at ~0.18 V in the cyclic voltammograms (CVs). This electrochemical polymerization process was stopped once the peak current has reached about 1.0 mA (Figure S2 in the Supporting Information). For comparison, PANI was also electrodeposited on stainless steel (SS, 304) sheets to obtain the PANI/SS composite films in the same manner and under identical conditions. Typical CVs during the electrodeposition of PANI onto WO₃ films or SS sheets are shown in Figure S2 in the Supporting Information.

Characterization. The morphologies of the samples were investigated by a Hitachi S4800 field emission scanning electron microscope (FE-SEM) at an accelerating voltage of 15.0 kV. X-ray diffraction (XRD) measurements were carried out by using a Bruker D8 Advance diffractometer with a Cu-K α radiation in the 2θ range of 10–90°. For the X-ray photoelectron spectroscopy (XPS) analysis, PHI Quantera X-ray photoelectron spectrometer with an Al cathode ($h\nu = 1486.6$ eV) as the X-ray source was used to examine the chemical states of W 4f electron and N 1s electron in the PANI/WO₃ films. Fourier transform infrared (FT-IR) spectra were collected on a Thermo Fisher Nicolet iS10 spectrometer by using a diamond attenuated total reflectance (ATR) accessory in the range of 1800–600 cm⁻¹ at a resolution of 4 cm⁻¹. The CVs of the composite film samples with active area of 2 cm² were recorded in various solutions with pH values of 1, 4, 7, and 10 over a potential range from -0.4 to 0.7 V to avoid oxidative degradation of PANI. The scan rate was 100 mV s⁻¹ unless otherwise stated.

RESULTS AND DISCUSSION

Morphology and Composition Studies. Figure 1 shows the SEM images of the surfaces of the WO₃ film and SS substrate, as well as the corresponding PANI/WO₃ and PANI/SS films. The WO₃ film formed by anodization in this work shows no nanoscale features except for some irregular pits (Figure 1a), which differs greatly from the nanopore structures reported by Schmuki and co-workers.³⁷ This difference in microscopic morphology may be attributed to the difference of the anodization temperatures, considering that their anodization experiments were conducted at lower temperatures (~4 °C).³⁷ In addition, the SS substrate also displays a flat featureless surface. Although WO₃ is a wide bandgap semiconductor, unlike TiO₂ film,³⁵ electrochemical polymerization of aniline is relatively easy to achieve on this electrode (Figure S2a in the Supporting Information). From Figure 1, it is evident that the PANI films on either the WO₃ film or SS

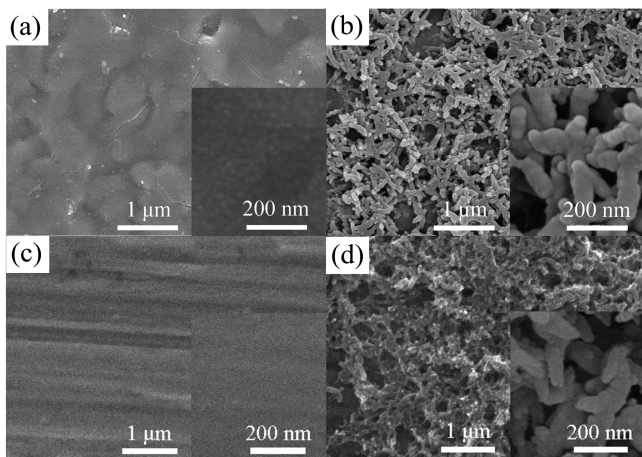


Figure 1. SEM images of (a) WO_3 film, (b) PANI/ WO_3 film, (c) SS sheet, and (d) PANI/SS film, respectively. Insets: the corresponding magnified images.

substrate show a nanofibrillar morphology, which is in agreement with the previous findings.³⁸ These PANI nanofibers form a three-dimensional porous network structure on the surface of the WO_3 film or SS substrate. This porous network structure should help to hinder the diffusion of H^+ ions within PANI film into the bulk solution.

Figure 2 shows typical XRD patterns of the PANI/ WO_3 film and the PANI/SS film, respectively. The XRD patterns of the WO_3 film and SS sheet are also given for comparison. All peaks for the annealed WO_3 film can be indexed to monoclinic WO_3 phase (JCPDS 88-545) except for the peaks at 40.14° , 58.16° , and 73.09° originated from W metal substrates. The XRD pattern of the PANI/ WO_3 film is quite similar to that of the WO_3 film, other than the slightly weakened intensity of the characteristic peaks. The crystal structure of the WO_3 film is not affected by the electrodeposition of PANI on it. For the PANI/SS film, no obvious diffraction peaks can be observed except for some peaks originated from the SS metal substrate (Figure 2b), revealing the amorphous structure of PANI deposited on the SS substrate. Similarly, the intensity of characteristic peaks for the SS substrate is also slightly reduced after the electrodeposition of PANI. These results exclude the possibility of the strong interactions between PANI chains and WO_3 molecules.

To confirm the chemical structure of the PANI deposited on the SS substrate and WO_3 film, we carried out FT-IR

spectroscopic studies. Figure 3 compares the FT-IR spectra of SS, PANI/SS, WO_3 , and PANI/ WO_3 films. As a control

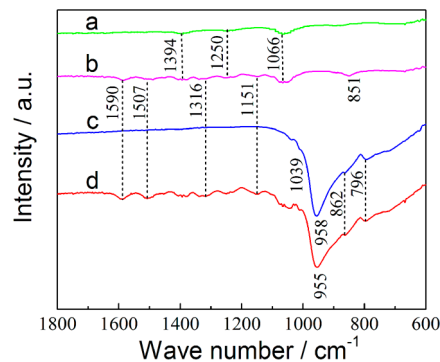


Figure 3. FT-IR spectra of (a) SS, (b) PANI/SS, (c) WO_3 film, and (d) PANI/ WO_3 film.

sample, the SS exhibits only three peaks at 1394 , 1250 , and 1066 cm^{-1} . For the PANI/SS film, except for the three peaks originated from the SS substrate, all other peaks can be assigned to PANI. The peaks at 1500 and 1507 cm^{-1} are ascribed to the stretching mode of the characteristic C–C in the quinoid and benzenoid rings, respectively. The peak at 1316 cm^{-1} corresponds to the C–N stretching vibration, which is characteristic in proton-doped PANI. The peaks at 1151 and 851 cm^{-1} are due to the in-plane bending of C–H in the quinoid ring and out-of-plane bending of C–H in the benzenoid ring. With respect to bare WO_3 film, a weak peak at about 1039 cm^{-1} is ascribed to the stretching mode of $\text{W}=\text{O}$ groups. The peak at 958 cm^{-1} is also attributed to the asymmetric vibration of $\text{W}=\text{O}$ bonds. The peaks at 862 and 796 cm^{-1} originate from the stretching mode of $\text{W}–\text{O}–\text{W}$ in WO_3 . While PANI was deposited on WO_3 film to form the PANI/ WO_3 composite film, the peaks in the range of 796 – 1039 cm^{-1} corresponding to WO_3 structures are virtually identical to each other between the bare WO_3 film and the PANI/ WO_3 film considering that the shifts are well within the 4 cm^{-1} resolution used for data acquisition. Like the PANI/SS film, the PANI/ WO_3 film also exhibits PANI characteristic peaks in the range of 1151 – 1500 cm^{-1} . The corresponding peak locations are not changed with respect to the PANI/SS film. No observed peak shifts for both PANI and WO_3 indicate the absence of the chemical interaction between the PANI film and the WO_3 matrix, which is consistent with the above result of XRD studies.

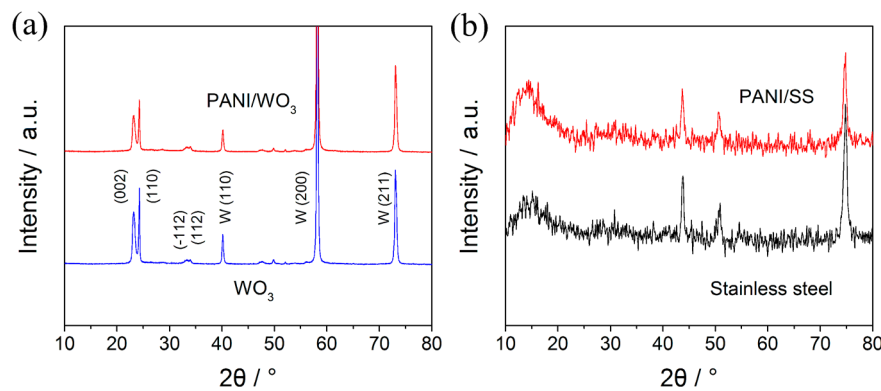


Figure 2. XRD patterns of (a) PANI/ WO_3 and (b) PANI/SS.

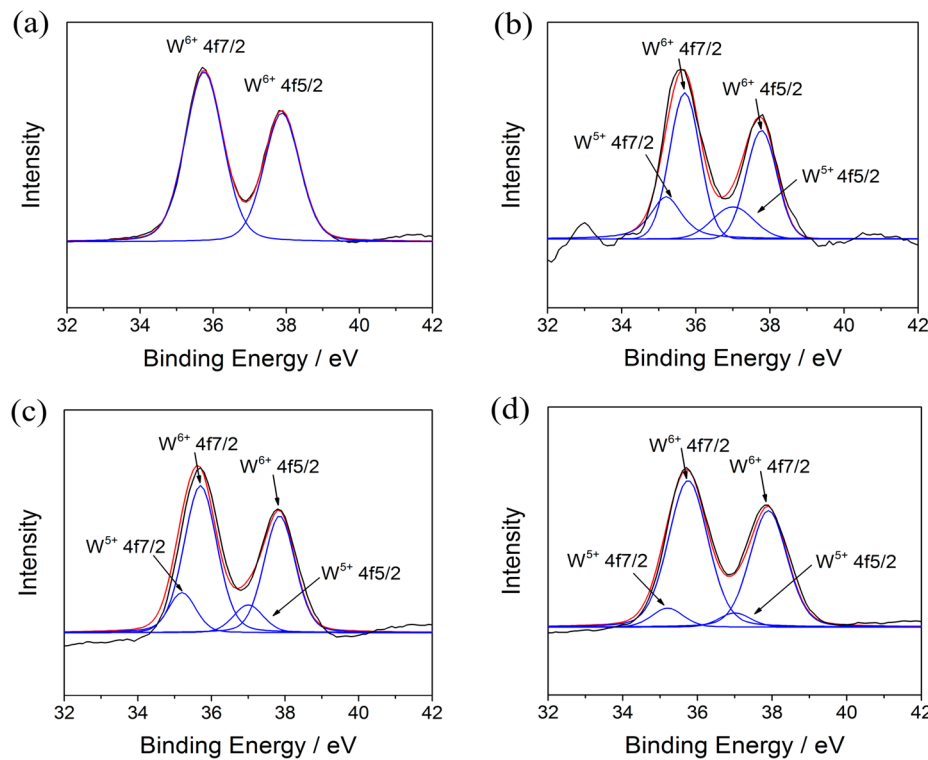


Figure 4. XPS spectra of W 4f: (a) WO₃ film, (b) PANI/WO₃ film before cycling, (c) PANI/WO₃ film after 30 cycles, and (d) PANI/WO₃ film after 500 cycles.

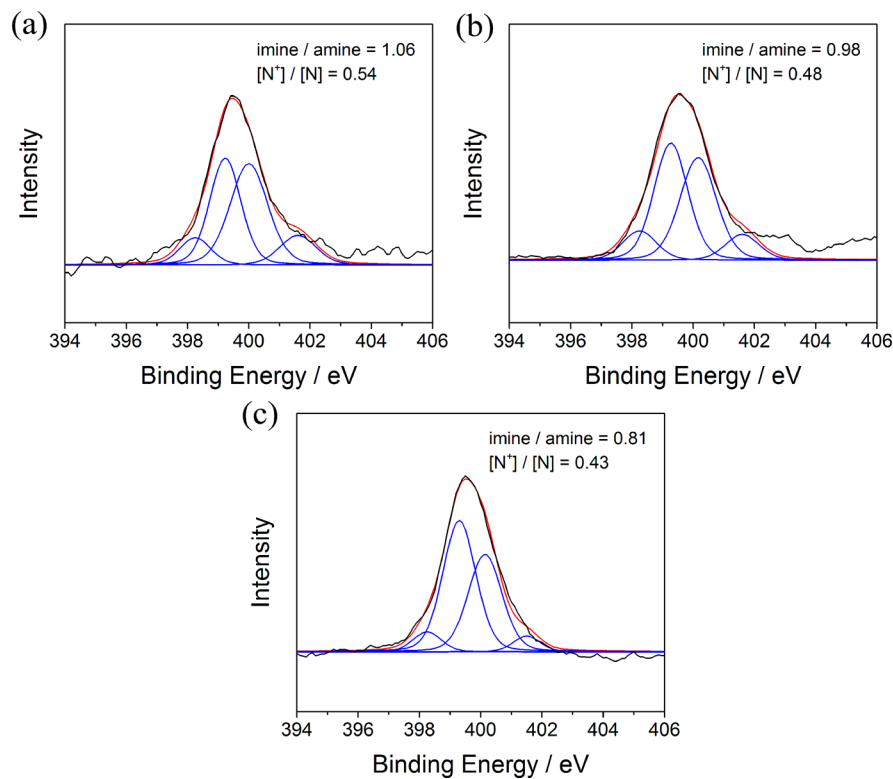


Figure 5. XPS spectra of N 1s: (a) PANI/WO₃ film before cycling, (b) PANI/WO₃ film after 30 cycles, and (c) PANI/WO₃ film after 500 cycles.

In order to examine the change in the chemical composition of the PANI/WO₃ films during the following cycling test, XPS measurements were performed. The XPS core level spectra of W 4f are shown in Figure 4. Peaks in all cases after the subtraction of a Shirley-type background were fitted using 20%

Gaussian curves. From Figure 4a, the well-resolved doublet peaks appearing at 35.7 and 37.9 eV assigned to W 4f_{7/2} and W 4f_{5/2} are associated with W⁶⁺ oxidation state, having a 4:3 f_{7/2}:f_{5/2} ratio and 2.2 eV f_{7/2}–f_{5/2} separation.³⁹ This indicates that the anodic tungsten oxide prepared in this

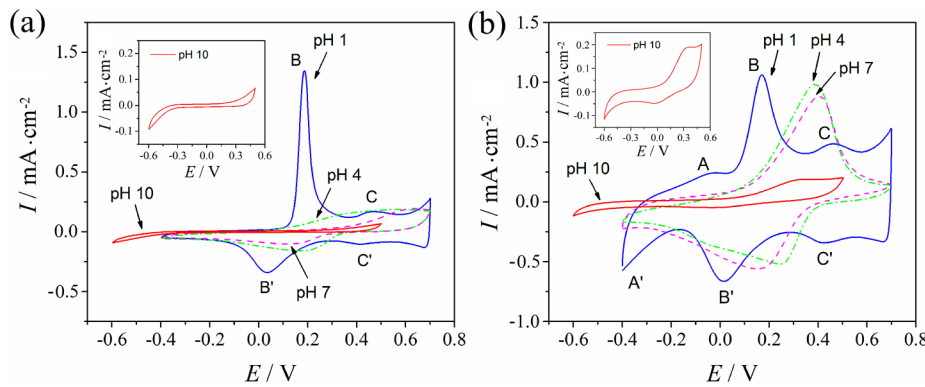


Figure 6. Second-cycle CVs for (a) PANI/SS film and (b) PANI/WO₃ film at a scan rate of 100 mV s⁻¹ in 0.1 M H₂SO₄ (pH 1), 0.5 M Na₂SO₄/0.5 M H₂SO₄ (pH 4), 0.5 M Na₂SO₄/0.1 M NaOH (pH 7), and 0.5 M Na₂SO₄/1.0 M NaOH (pH 10), respectively. Insets: the enlarged CVs at pH 10.

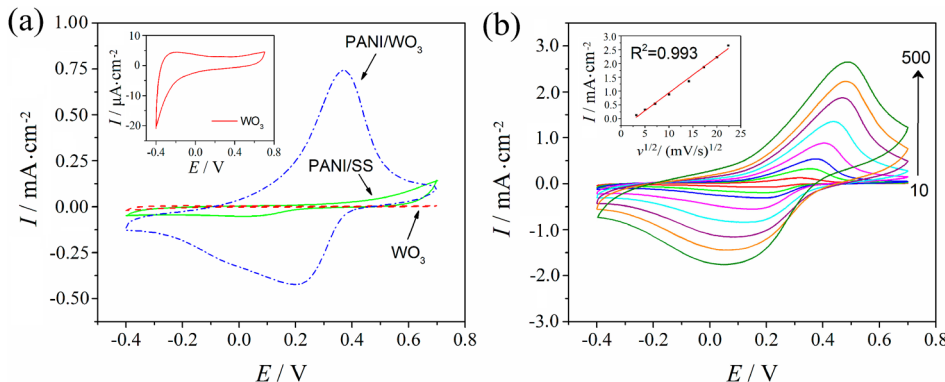


Figure 7. (a) Tenth-cycle CVs of PANI/WO₃, PANI/SS, and WO₃ films in pH 7 Na₂SO₄ solution. Inset: the enlarged CV of the WO₃ film. (b) The second-cycle CVs of PANI/WO₃ film in pH 7 Na₂SO₄ solution recorded at various scan rates (from inner to outer) of 10, 25, 50, 100, 200, 300, 400, and 500 mV s⁻¹. Inset: the relationship between the anodic peak current and the square root of the scan rate.

work is WO₃ film. As for the PANI/WO₃ films in different stages of the cycling test (Figure 4b–d), the weak doublet peaks located at 35.2 and 37.0 eV assigning to W 4f7/2 and W 4f5/2 are all visible, diagnosing the presence of W⁵⁺ oxidation state.⁴⁰ The W⁵⁺ in the PANI/WO₃ films results from the W⁶⁺ reduction, which is assisted by H⁺ intercalation from the electrolyte as charge compensation. Moreover, the intensity ratio of W⁵⁺/W⁶⁺ decreases with increasing cycle, implying that the W⁵⁺ concentration in WO₃ layer of the PANI/WO₃ films decreases gradually during cycling.

The N 1s core level peak can be deconvoluted into four peaks, as shown in Figure 5. The peaks at 398.2 and 399.3 eV are associated with undoped imine units (−N=) and undoped amine units (−NH−).⁴¹ In contrast, the peak at 400.0 eV can be assigned to protonated imine units (−N⁺=) and the peak at 401.6 eV is proposed to correlate with protonated amine units (−NH⁺).⁴¹ Imine/amine ratios, which could be associated with the oxidation state, were estimated by the sum of the corresponding peak areas (i.e., sum of −NH− and −NH⁺−/sum of −N= and −N⁺=). [N⁺]/[N] ratios, which could be correlated with the doping level, were determined by the area ratios of the peaks ([N⁺], sum of −N⁺= and −NH⁺−; [N], sum of −N=, −NH−, −N⁺=, and −NH⁺−). The calculated values of imine/amine ratios and [N⁺]/[N] ratios for the PANI/WO₃ films upon cycling are also listed in Figure 5. It is seen that the imine/amine ratio is close to 1 in the initial period of cycling, indicating that the PANI in the PANI/WO₃ films is in the emeraldine oxidation state. However, this value falls down to 0.81 after 500 cycles, implying that some amine units

have not been reduced fully during the cycling test. This phenomenon corresponds to the decreased [N⁺]/[N] ratios, which can be ascribed to the reduced content of H⁺ in the PANI/WO₃ films (discussed below).

Electrochemical Activity at Different pH Values. Figure 6 presents the CVs for the PANI/SS and PANI/WO₃ films in solutions of various pH values. As can be seen from Figure 6a, an increase in solution pH leads to a loss of electroactivity of PANI for the PANI/SS film. PANI in the PANI/SS film shows good electroactivity only in a pH 1 solution, two redox couples (B/B', C/C') at 0.19 V/0.04 V and 0.47 V/0.42 V in the CV can be clearly observed, which correspond to the transitions between leucoemeraldine salt (LS)/emeraldine salt (ES) and emeraldine salt (ES)/pernigraniline salt (PS), respectively.³² In the media of pH 7 and pH 10, PANI lost its electroactivity completely. At pH 4, only a pair of very weak and broad redox peaks can be found. These results indicate that the prepared PANI film on SS substrate can retain its electroactivity only at pH < 4, which is consistent with previous studies.¹¹ On the contrary, for the PANI/WO₃ film, it is clear from Figure 6b that PANI can remain the redox activity at pH value up to 10. At pH 1, the CV displays three pairs of redox peaks within the applied potential window. The redox couple A/A' at −0.03 V/−0.4 V can be attributed to the intercalation/deintercalation of protons (H⁺) and electrons (e[−]) into/out of the WO₃ film.^{26,42} The other two redox couples, B/B' at 0.17 V/0.01 V and C/C' at 0.47 V/0.42 V, result from the transitions between LS/ES and ES/PS of PANI, respectively. That is, in the strongly acidic solution, the PANI/WO₃ film exhibits both characteristic peaks

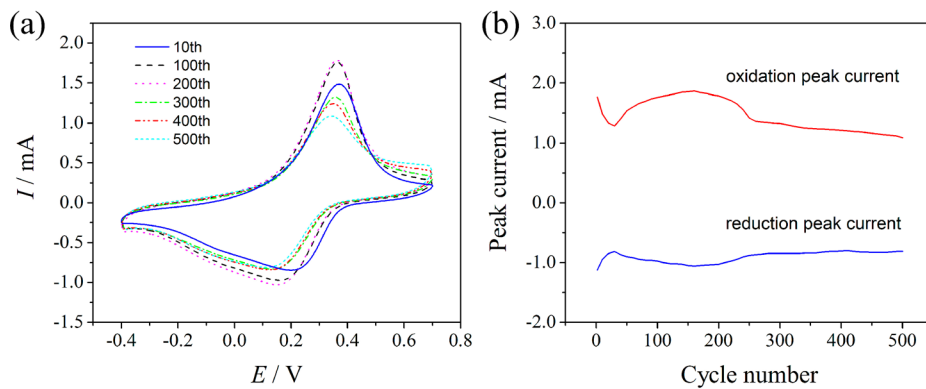


Figure 8. (a) CVs of the PANI/WO₃ film in pH 7 Na₂SO₄ solution corresponding to different potentiodynamic cycles. (b) The corresponding peak current evolution of PANI/WO₃ film during cycling.

of PANI and WO₃, in good agreement with previous findings.^{26,27}

In addition, the peak potentials of two redox couples (B/B', C/C') for the PANI/WO₃ film are approximately identical to those of the corresponding redox couples for the PANI/SS film, implying that the presence of WO₃ has little influence on the electrochemical characteristics of PANI. This result also excludes the possibility for the existence of interactions between the PANI and WO₃ phases, in accordance with the results of XRD and FT-IR spectroscopy studies.

Interestingly, unlike the PANI/SS film, the PANI/WO₃ film still possesses stable electroactivity at higher pH values. At pH 4 and pH 7, the PANI/WO₃ film exhibits distinct redox peaks as shown in Figure 6b. Nevertheless, only one pair of redox peaks can be observed at these higher pH values instead of three redox couples occurring at pH 1. Even at pH value up to 10, well-defined oxidation and reduction peaks for the PANI/WO₃ film can also be seen, although the peak currents are visibly reduced compared with those at pH 4 and pH 7, indicating that it is still electroactive at this pH. In addition, the peak-to-peak separation becomes larger with increasing pH (Figure 6b), which is similar to those found for the polymer acid-doped PANI.²² The results reveal that the WO₃ support can extend the electroactivity of PANI from acidic to neutral and even slightly alkaline solutions.

Electrochemical Activity at pH 7. Considering that this study is aimed at extending the applicability of PANI to higher pH environment (e.g., for biosensor applications), we focus our attention on the electrochemical behaviors of the PANI/WO₃ film in neutral solutions in the following section. Figure 7a compares the tenth-cycle CVs of the PANI/WO₃, PANI/SS, and WO₃ films in pH 7 Na₂SO₄ solution. Clearly, only the PANI/WO₃ film exhibits significantly high peak currents in the neutral solution, exhibiting one oxidation peak at 0.38 V and two reduction peaks at 0.20 and -0.08 V. Since the current response of the WO₃ film at pH 7 is very low (inset of Figure 7a), these redox peaks should be attributed to two redox processes (LS/ES and ES/PS) of the PANI state or their overlap.^{43,44} Moreover, from the CVs, the ratio between anodic charge (2.04 mQ/cm²) and cathodic charge (1.94 mQ/cm²) can be estimated as 1.05 for the PANI/WO₃ film, implying a high degree of redox reversibility at pH 7. By comparison, for the PANI/SS film, this ratio between anodic charge (0.19 mQ/cm²) and cathodic charge (0.25 mQ/cm²) is 0.76, markedly less than 1. Figure 7b shows the CVs of the PANI/WO₃ film in pH 7 Na₂SO₄ electrolyte at different scan rates. As the scan rate

increases, the oxidation peak slightly shifts toward a more positive potential and the reduction peak toward a more negative potential. While the anodic peak currents are plotted against the square root of the scan rate ($v^{1/2}$), as presented in the inset, a good linear relationship can be obtained, suggesting that the redox reaction is a diffusion-controlled process.⁴⁴

To examine the redox stability of the PANI/WO₃ film in the neutral solution, it was subjected to 500 potentiodynamic cycles (~3 h) at a scan rate of 100 mV s⁻¹. Figure 8 shows its CVs and redox peak current evolution during cycling. Only some representative CVs for 500 consecutive cycles are presented in Figure 8a for clarity. As a whole, the shape of the CVs and peak potentials remain relatively unchanged over 500 cycles. This demonstrates that the electroactivity of the PANI/WO₃ film at pH 7 is very stable and reversible toward repeated cycling, which are important aspects for practical applications. Unfortunately, the cycling stability of PANI electroactivity at higher pH values was seldom reported in the previous studies as mentioned above, especially for long periods of cycling. In addition, the PANI/WO₃ film exhibits a complicated behavior for the evolution of oxidation and reduction peak currents with cycle number as shown in Figure 8b. In the initial period of cycling (~30 cycles), the oxidation and reduction peak currents display a fast decay. Then, it is surprising that the peak currents begin to increase remarkably with cycle number until a maximum value is reached after ~170 cycles. Thereafter, the peak currents tend to decrease gradually over the following cycles. The oxidation peak current still retains 58% of its maximum value after 500 cycles, suggesting extremely stable electroactivity in the neutral solution. By contrast, for the poly(acrylic acid)-doped PANI, a similar attenuation of the redox peak currents can be observed only after 20 cycles.²²

Evidently, the excellent electroactivity of the PANI/WO₃ film at pH 7 is closely related to the underlying WO₃ substrate. Note that the electrodeposition of PANI onto the WO₃ film was carried out by cyclic voltammetry in an acidic solution containing 0.5 M H₂SO₄. Therefore, the deposited PANI is in doped ES form, which has been confirmed by the preceding FT-IR spectroscopy and XPS analyses. Further, as illustrated in eq 1, the W⁶⁺/W⁵⁺ redox process in the underlying WO₃ film, accompanied by a concomitant intercalation/deintercalation of H⁺ into/out of the film, might occur simultaneously during the electrodeposition of PANI, which can be verified by the presence of reduction peak in CVs recorded for the electropolymerization of aniline on the WO₃ film (Figure S2a in the Supporting Information). This resulted in the residual of

H^+ in the underlying WO_3 film after the PANI electro-deposition, which was supported indirectly by the presence of W^{5+} inside the film detected by XPS (Figure 4b). It is believed that these intercalated H^+ ions in WO_3 film act as proton sources for PANI, leading to the excellent electroactivity and high redox stability of PANI in neutral media.

As schematically illustrated in Figure 9, during the potential sweep in the anodic direction, H^+ ions intercalated into WO_3

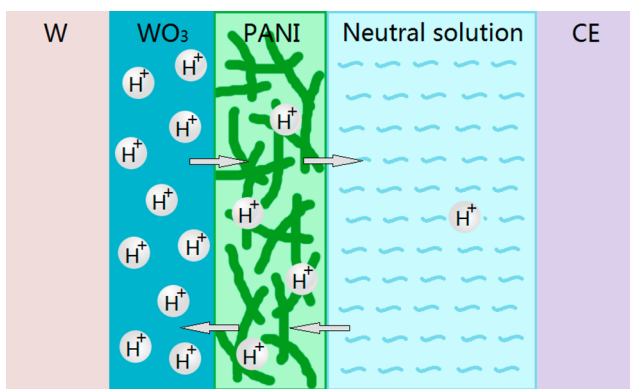


Figure 9. Schematic illustration of H^+ transport processes in PANI/ WO_3 system during cycling.

layer can enter PANI layer through the WO_3 –PANI interface due to the W^{5+} oxidation (eq 1). However, H^+ ions within PANI layer tend to diffuse into the neutral solution across the PANI–solution interface owing to H^+ concentration gradients at the interface. The latter process causes a continuous loss of H^+ ions within PANI layer upon cycling, thereby destroying the electroactivity of PANI. This is the case for the PANI/SS film. However, for the PANI/ WO_3 film, while the potential scan is reversed (toward negative potentials), H^+ ions can return back to the WO_3 side because of the action of an electric field and the reduction of WO_3 (accompanied by the intercalation of H^+ ions). It is the presence of the reverse process that partially balances the loss of H^+ ions in the PANI layer and thus maintains the electroactivity of PANI at pH 7 during cycling.

At the beginning of the repeated cycling test, the diffusion of H^+ ions into the bulk solution at the PANI–solution interface is dominant because of a steep concentration gradient of H^+ at the interface, whereas at WO_3 –PANI interface, the supply rate of H^+ ions released from the WO_3 film to PANI layer is likely to be lower than that of H^+ diffusion toward the bulk solution. The net result is a decrease in H^+ concentration in the PANI

layer, giving rise to a marked decrease in redox peak currents in the initial period of cycling (Figure 8b). As the cycling continues further, the diffusion rate of H^+ ions into the bulk solution should be slowed down gradually to reach a minimum because the concentration gradient of H^+ at the PANI–solution interface will be reduced to a steady-state value over a period of time. In this case, the supply rate of H^+ ions released from the WO_3 film to PANI layer can exceed the diffusion rate of H^+ ions into the bulk solution. As a result, H^+ concentration in the PANI layer will increase gradually during cycling, leading to an enhancement of PANI electroactivity. This explains why the peak currents can surprisingly increase with cycle number after a short decline period. Given that there is a general tendency for H^+ ions to enter the neutral solution, the H^+ ions incorporated in WO_3 layer would be lost slowly during cycling. Accordingly, while the amount of H^+ ions released from WO_3 layer is eventually less than that diffused into the solution, the net concentration of H^+ ions in the PANI layer starts to decrease, which in turn results in a decrease in electroactivity of PANI. This corresponds to the descending period of the peak currents in Figure 8b after reaching a maximum. In addition, the XPS data showed that the W^{5+} concentration in WO_3 layer of the PANI/ WO_3 film decreases gradually during cycling (Figure 4). According to eq 1, the amount of the corresponding H^+ ions within WO_3 layer should also be reduced during cycling, which is in good agreement with the above discussion.

As described above, the H^+ ions within WO_3 layer can enter PANI layer by deintercalation when scanning toward anodic potential. The amount of the deintercalated H^+ ions is certainly influenced by the scan rate for the partially reversible redox systems. It is, therefore, not surprising that the cycling behavior of the PANI/ WO_3 film in the neutral solution would be altered while changing the scan rate. Figure 10 displays the consecutive CVs of the PANI/ WO_3 film recorded in the neutral solution at scan rates of 10 and 500 mV s⁻¹, respectively. It can be seen that at a lower scan rate (10 mV s⁻¹) the response of redox currents is always improving during cycling, and the second oxidation peak (at a more positive potential), which is absent at 100 mV s⁻¹, becomes observable gradually. Conversely, at a higher scan rate (500 mV s⁻¹), the response of redox currents is always decreasing and the oxidation peaks appear at a slightly positive shift upon cycling. As already discussed above, at the lower scan rate, the more H^+ ions can be deintercalated into PANI layer accompanied by the W^{5+} oxidation during scanning toward anodic potential. Consequently, the H^+ ion flux into PANI layer is probably higher than that of H^+ diffusion toward

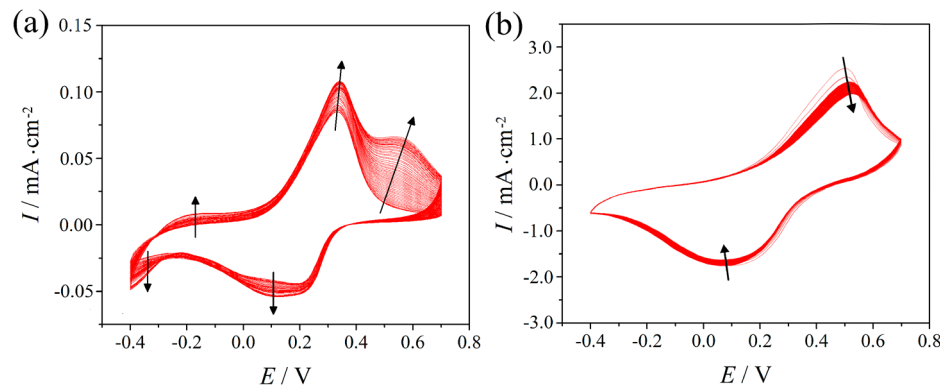


Figure 10. Consecutive CVs of the PANI/ WO_3 film in pH 7 Na_2SO_4 solution at scan rates of (a) 10 and (b) 500 mV s⁻¹ for 60 cycles.

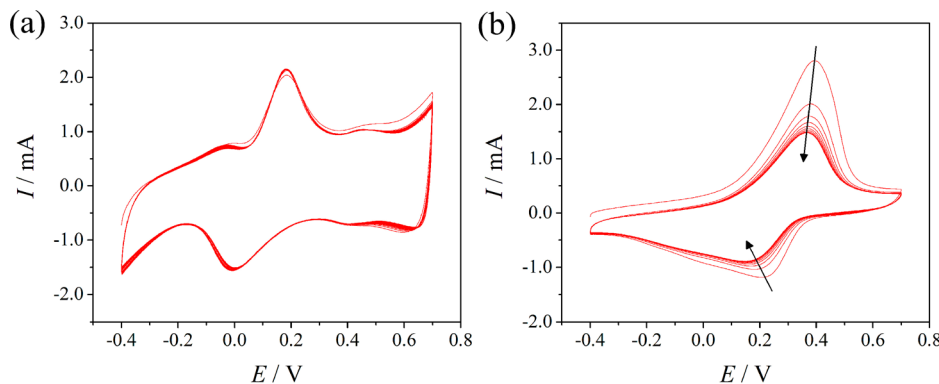


Figure 11. (a) Consecutive CVs of the PANI/WO₃ sample, which was subjected to 500 cycles in pH 7 solution, recorded in 0.1 M H₂SO₄ at 100 mV s⁻¹ for 20 cycles. (b) Consecutive CVs recorded in pH 7 Na₂SO₄ solution at 100 mV s⁻¹ for 10 cycles.

the bulk solution at the beginning of cycling, despite the prolonged diffusion time for H⁺ ions at the lower scan rate. This leads to a continuous increase in the redox peak currents (Figure 10a). Moreover, since the net concentration of H⁺ ions in the PANI layer is increasing during cycling, the second oxidation peak, which corresponds to the transitions between ES and PS and is highly pH-dependent,^{44,45} becomes more and more dominant. Of course, the slow scan rate may also facilitate this oxidation process. On the contrary, at the higher scan rate, the amount of H⁺ ions into PANI layer would be reduced because of the slower deintercalation kinetics during sweeping anodically compared with that at 100 mV s⁻¹. Thus, the H⁺ ion flux into PANI layer is always lower than that of H⁺ diffusion toward the bulk solution, resulting in a continuous decrease in redox peak currents owing to the reduced concentration of H⁺ ions in the PANI layer during cycling.

On the basis of the above analyses, one can infer that the intercalated H⁺ ions in WO₃ film as the proton supplier play a significant role in electroactivity of PANI in neutral media. To further confirm this idea, we tried to eliminate the intercalated H⁺ ions in the PANI/WO₃ sample after the cycling test of 500 cycles by exceeding 12 h of continuous immersion in 0.5 M Na₂SO₄ (pH 7). As expected, redox peaks in the CVs disappear completely in neutral media, as seen in Figure S3 in the Supporting Information, indicating the severe damage of its electrochemical activity. However, when the same sample without any electroactivity was subjected to 20 potentiodynamic cycles in an acidic solution, redox peaks emerged again in the recorded CVs as shown in Figure 11a due to the protonic acid redoping of PANI. Furthermore, the CVs in Figure 11a are very similar to the corresponding CV (at pH 1) in Figure 6b, also exhibiting the redox couple, which can be assigned to the intercalation/deintercalation of protons into/out of the WO₃ film. This result indicates that the H⁺ ions were intercalated into WO₃ film again by the potentiodynamic cycling in the acidic solution. Thus, the PANI/WO₃ sample by this treatment should restore its redox activity at pH 7. Figure 11b confirms this expectation, where the treated PANI/WO₃ sample exhibits remarkable redox peaks in pH 7 solution, with almost no observable changes in both the peak currents and the peak potentials in comparison with those in Figure 8a. This experimental result not only demonstrates the above mechanisms for achieving good electroactivity but also provides an effective method to restore the electroactivity of the PANI/WO₃ film, which is very attractive for practical applications.

CONCLUSIONS

In this study, PANI was electrodeposited onto the surface of anodic WO₃ film by cyclic voltammetry. For the first time, we found that the as-prepared PANI/WO₃ film exhibits an excellent electrochemical activity and high cycling stability in neutral media. In the PANI/WO₃ system, the WO₃ film serves as a host for H⁺ insertion, which can provide proton sources for PANI and make PANI electroactive at higher pH values. This method to shift the electroactivity of PANI beyond pH 7 is conceptually new from the previous strategies, which can offer an innovative protocol to enhance the electroactivity of PANI in neutral solutions. Moreover, the deterioration of electroactivity for the PANI/WO₃ film over long periods of continuous immersion in a neutral solution can be recovered readily by cyclic voltammetry in an acidic solution. The present results should open new perspectives for the application of PANI in high pH environments.

ASSOCIATED CONTENT

Supporting Information

Anodizing current transients of W foils, and cyclic voltammograms of the electropolymerization of aniline and the PANI/WO₃ film after immersing for 12 h. This material is available free of charge via the Internet at <http://pubs.acs.org>.

AUTHOR INFORMATION

Corresponding Authors

*E-mail: lidd@sari.ac.cn.

*E-mail: soong_ye@sohu.com.

Notes

The authors declare no competing financial interest.

ACKNOWLEDGMENTS

This work was supported financially by the National Natural Science Foundation of China (Grant Nos. 51077072, 51377085, and 61171043) and Science and Technology Commission of Shanghai Municipality (14JC1492900).

REFERENCES

- (1) Kang, E. T.; Neoh, K. G.; Tan, K. L. Polyaniline: A Polymer with Many Interesting Intrinsic Redox States. *Prog. Polym. Sci.* **1998**, *23*, 277–324.
- (2) Chan, H. S. O.; Ng, S. C.; Ho, P. K. H. Polyanilines Doped with Phosphonic Acids: Their Preparation and Characterization. *Macromolecules* **1994**, *27*, 2159–2164.

- (3) Tai, Q.; Chen, B.; Guo, F.; Xu, S.; Hu, H.; Sebo, B.; Zhao, X. Z. In Situ Prepared Transparent Polyaniline Electrode and Its Application in Bifacial Dye-Sensitized Solar Cells. *ACS Nano* **2011**, *5*, 3795–3799.
- (4) DeLongchamp, D. M.; Hammond, P. T. Multiple-Color Electrochromism from Layer-by-Layer-Assembled Polyaniline/Prussian Blue Nanocomposite Thin Films. *Chem. Mater.* **2004**, *16*, 4799–4805.
- (5) Huang, J.; Virji, S.; Weiller, B. H.; Kaner, R. B. Polyaniline Nanofibers: Facile Synthesis and Chemical Sensors. *J. Am. Chem. Soc.* **2003**, *125*, 314–315.
- (6) Wang, H.; Hao, Q.; Yang, X.; Lu, L.; Wang, X. Effect of Graphene Oxide on the Properties of Its Composite with Polyaniline. *ACS Appl. Mater. Interfaces* **2010**, *2*, 821–828.
- (7) Wei, H.; Gu, H.; Guo, J.; Wei, S.; Guo, Z. Electropolymerized Polyaniline Nanocomposites from Multi-Walled Carbon Nanotubes with Tuned Surface Functionalities for Electrochemical Energy Storage. *J. Electrochem. Soc.* **2013**, *160*, G3038–G3045.
- (8) Miao, Y. E.; Fan, W.; Chen, D.; Liu, T. High-Performance Supercapacitors Based on Hollow Polyaniline Nanofibers by Electrospinning. *ACS Appl. Mater. Interfaces* **2013**, *5*, 4423–4428.
- (9) Wei, H.; Zhu, J.; Wu, S.; Wei, S.; Guo, Z. Electrochromic Polyaniline/Graphite Oxide Nanocomposites with Endured Electrochemical Energy Storage. *Polymer* **2013**, *54*, 1820–1831.
- (10) Wei, H.; Gu, H.; Guo, J.; Wei, S.; Liu, J.; Guo, Z. Silica Doped Nanopolyaniline with Endured Electrochemical Energy Storage and the Magnetic Field Effects. *J. Phys. Chem. C* **2013**, *117*, 13000–13010.
- (11) Diaz, A. F.; Logan, J. A. Electroactive Polyaniline Films. *J. Electroanal. Chem. Interfacial Electrochem.* **1980**, *111*, 111–114.
- (12) Tian, S.; Liu, J.; Zhu, T.; Knoll, W. Polyaniline/Gold Nanoparticle Multilayer Films: Assembly, Properties, and Biological Applications. *Chem. Mater.* **2004**, *16*, 4103–4108.
- (13) Song, Y.; Lv, H.; Hu, S.; Yang, C.; Zhu, X. Electroactivity of Polyaniline in High pH Solutions. *Acta Chim. Sin.* **2013**, *71*, 999–1006.
- (14) Yue, J.; Epstein, A. J. Synthesis of Self-Doped Conducting Polyaniline. *J. Am. Chem. Soc.* **1990**, *112*, 2800–2801.
- (15) Yamamoto, K.; Taneichi, D. A Self-Doped Oligoaniline with Two Stable Redox Couples in a Wide pH Range. *Macromol. Chem. Phys.* **2000**, *201*, 6–11.
- (16) Zhang, L. Electrochemical Synthesis of Self-Doped Polyaniline and Its Use to the Electrooxidation of Ascorbic Acid. *J. Solid State Electrochem.* **2007**, *11*, 365–371.
- (17) Bian, L. J.; Luan, F.; Liu, S. S.; Liu, X. X. Self-Doped Polyaniline on Functionalized Carbon Cloth as Electroactive Materials for Supercapacitor. *Electrochim. Acta* **2012**, *64*, 17–22.
- (18) Tarver, J.; Yoo, J. E.; Dennes, T. J.; Schwartz, J.; Loo, Y. L. Polymer Acid Doped Polyaniline Is Electrochemically Stable Beyond pH 9. *Chem. Mater.* **2008**, *21*, 280–286.
- (19) Zhou, H.; Lin, Y.; Yu, P.; Su, L.; Mao, L. Doping Polyaniline with Pristine Carbon Nanotubes into Electroactive Nanocomposite in Neutral and Alkaline Media. *Electrochim. Commun.* **2009**, *11*, 965–968.
- (20) Coşkun, E.; Zaragoza-Contreras, E. A.; Salavagione, H. J. Synthesis of Sulfonated Graphene/Polyaniline Composites with Improved Electroactivity. *Carbon* **2012**, *50*, 2235–2243.
- (21) Feng, X.; Mao, C.; Yang, G.; Hou, W.; Zhu, J. J. Polyaniline/Au Composite Hollow Spheres: Synthesis, Characterization, and Application to the Detection of Dopamine. *Langmuir* **2006**, *22*, 4384–4389.
- (22) Bartlett, P. N.; Simon, E. Poly(aniline)-Poly(acrylate) Composite Films as Modified Electrodes for the Oxidation of NADH. *Phys. Chem. Chem. Phys.* **2000**, *2*, 2599–2606.
- (23) Zhang, H.; Zong, R.; Zhu, Y. Photocorrosion Inhibition and Photoactivity Enhancement for Zinc Oxide via Hybridization with Monolayer Polyaniline. *J. Phys. Chem. C* **2009**, *113*, 4605–4611.
- (24) Sharma, B. K.; Gupta, A. K.; Khare, N.; Dhawan, S. K.; Gupta, H. C. Synthesis and Characterization of Polyaniline-ZnO Composite and Its Dielectric Behavior. *Synth. Met.* **2009**, *159*, 391–395.
- (25) Jiang, H.; Ma, J.; Li, C. Polyaniline-MnO₂ Coaxial Nanofiber with Hierarchical Structure for High-Performance Supercapacitors. *J. Mater. Chem.* **2012**, *22*, 16939–16942.
- (26) Zou, B. X.; Liu, X. X.; Diamond, D.; Lau, K. T. Electrochemical Synthesis of WO₃/PANI Composite for Electrocatalytic Reduction of Iodate. *Electrochim. Acta* **2010**, *55*, 3915–3920.
- (27) Janáky, C.; de Tacconi, N. R.; Chanmanee, W.; Rajeshwar, K. Electrodeposited Polyaniline in a Nanoporous WO₃ Matrix: An Organic/Inorganic Hybrid Exhibiting Both p-and n-Type Photoelectrochemical Activity. *J. Phys. Chem. C* **2012**, *116*, 4234–4242.
- (28) Zhang, J.; Tu, J. P.; Du, G. H.; Dong, Z. M.; Wu, Y. S.; Chang, L.; Xie, D.; Cai, G. G.; Wang, X. L. Ultra-Thin WO₃ Nanorod Embedded Polyaniline Composite Thin Film: Synthesis and Electrochromic Characteristics. *Sol. Energy Mater. Sol. Cells* **2013**, *114*, 31–37.
- (29) Ganeshan, R.; Gedanken, A. Organic-Inorganic Hybrid Materials Based on Polyaniline/TiO₂ Nanocomposites for Ascorbic Acid Fuel Cell Systems. *Nanotechnology* **2008**, *19*, 435709.
- (30) Xiong, S.; Phua, S. L.; Dunn, B. S.; Ma, J.; Lu, X. Covalently Bonded Polyaniline-TiO₂ Hybrids: A Facile Approach to Highly Stable Anodic Electrochromic Materials with Low Oxidation Potentials. *Chem. Mater.* **2010**, *22*, 255–260.
- (31) Tai, H.; Jiang, Y.; Xie, G.; Yu, J.; Chen, X. Fabrication and Gas Sensitivity of Polyaniline-Titanium Dioxide Nanocomposite Thin Film. *Sens. Actuators, B* **2007**, *125*, 644–650.
- (32) Wei, H.; Yan, X.; Wu, S.; Luo, Z.; Wei, S.; Guo, Z. Electropolymerized Polyaniline Stabilized Tungsten Oxide Nanocomposite Films: Electrochromic Behavior and Electrochemical Energy Storage. *J. Phys. Chem. C* **2012**, *116*, 25052–25064.
- (33) Wei, H.; Ding, D.; Yan, X.; Guo, J.; Shao, L.; Chen, H.; Sun, L.; Colorado, H. A.; Wei, S.; Guo, Z. Tungsten Trioxide/Zinc Tungstate Bilayers: Electrochromic Behaviors, Energy Storage and Electron Transfer. *Electrochim. Acta* **2014**, *132*, 58–66.
- (34) Lyon, L. A.; Hupp, J. T. Energetics of the Nanocrystalline Titanium Dioxide/Aqueous Solution Interface: Approximate Conduction Band Edge Variations between H₀ = -10 and H₋ = +26. *J. Phys. Chem. B* **1999**, *103*, 4623–4628.
- (35) Song, Y.; Lv, H.; Yang, C.; Xiao, H.; Chen, X.; Zhu, X.; Li, D. Enhanced Electroactivity at Physiological pH for Polyaniline in Three-Dimensional Titanium Oxide Nanotube Matrix. *Phys. Chem. Chem. Phys.* **2014**, *16*, 15796–15799.
- (36) Zheng, H.; Ou, J. Z.; Strano, M. S.; Kaner, R. B.; Mitchell, A.; Kalantar-zadeh, K. Nanostructured Tungsten Oxide-Properties, Synthesis, and Applications. *Adv. Funct. Mater.* **2011**, *21*, 2175–2196.
- (37) Hahn, R.; Macak, J. M.; Schmuki, P. Rapid Anodic Growth of TiO₂ and WO₃ Nanotubes in Fluoride Free Electrolytes. *Electrochim. Commun.* **2007**, *9*, 947–952.
- (38) Li, H.; Wang, J.; Chu, Q.; Wang, Z.; Zhang, F.; Wang, S. Theoretical and Experimental Specific Capacitance of Polyaniline in Sulfuric Acid. *J. Power Sources* **2009**, *190*, 578–586.
- (39) Baek, Y.; Yong, K. Controlled Growth and Characterization of Tungsten Oxide Nanowires Using Thermal Evaporation of WO₃ Powder. *J. Phys. Chem. C* **2007**, *111*, 1213–1218.
- (40) Lu, X.; Zhai, T.; Zhang, X.; Shen, Y.; Yuan, L.; Hu, B.; Gong, L.; Chen, J.; Gao, Y.; Zhou, J.; et al. WO_{3-x}@Au@MnO₂ Core–Shell Nanowires on Carbon Fabric for High-Performance Flexible Supercapacitors. *Adv. Mater.* **2012**, *24*, 938–944.
- (41) Wei, X. L.; Fahlman, M.; Epstein, A. J. XPS Study of Highly Sulfonated Polyaniline. *Macromolecules* **1999**, *32*, 3114–3117.
- (42) Kulesza, P. J.; Faulkner, L. R. Electrocatalysis at a Novel Electrode Coating of Nonstoichiometric Tungsten (VI,V) Oxide Aggregates. *J. Am. Chem. Soc.* **1988**, *110*, 4905–4913.
- (43) Bartlett, P. N.; Birkin, P. R.; Wallace, E. N. K. Oxidation of b-Nicotinamide Adenine Dinucleotide (NADH) at Poly(Aniline)-Coated Electrodes. *J. Chem. Soc., Faraday Trans.* **1997**, *93*, 1951–1960.
- (44) Tian, S.; Baba, A.; Liu, J.; Wang, Z.; Knoll, W.; Park, M. K.; Advincula, R. Electroactivity of Polyaniline Multilayer Films in Neutral Solution and Their Electrocatalyzed Oxidation of β -Nicotinamide Adenine Dinucleotide. *Adv. Funct. Mater.* **2003**, *13*, 473–479.

(45) Huang, W. S.; Humphrey, B. D.; MacDiarmid, A. G. Polyaniline, a Novel Conducting Polymer Morphology and Chemistry of its Oxidation and Reduction in Aqueous Electrolytes. *J. Chem. Soc., Faraday Trans.* **1986**, *82*, 2385–2400.